Quantum-Enhanced Imaging of Trapped Ions: Final Report

August 25, 2016

Robert McConnell, Colin Bruzewicz, Guang Hao Low, Theodore Yoder, Isaac Chuang, John Chiaverini and Jeremy Sage

Task Summary (Experimental)

All Tasks of the project are now complete. We have successfully demonstrated the essential aspects of quantum-enhanced imaging, including imaging resolution to within less than 10% of the beam width, scaling of the imaging resolution that approaches the Heisenberg limit, and implementation of the binary search algorithm for the trapped ion. The program accomplishments are described in more detail below. At the end of this report, we discuss the prospects for future work in this area.

Task 1

Stabilization of beam path and intensity fluctuations

We installed a test beam path to measure positional fluctuations of the beam. The beam was coupled into an optical fiber and then launched from an adjustable fiber collimator. Using a four-quadrant photodiode, we measured the positional fluctuations, shown below in Figure 1. The measurements indicated that the remaining angular fluctuations were below the 10^{-5} level. This corresponds to less than 2 um of positional error at the ion location (out of a beam waist of 100 um), sufficient for the program goals.

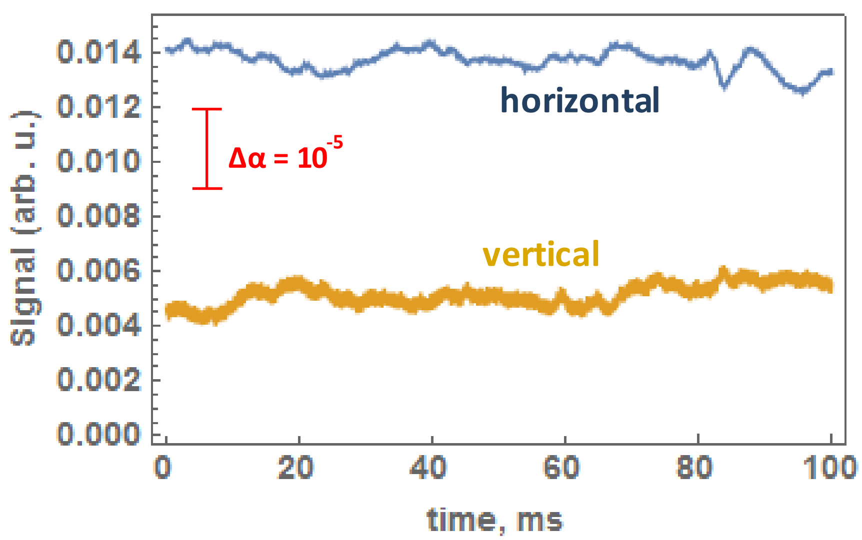

Figure 1. Horizontal and vertical positional fluctuation as measured in the test beam setup

Following completion of this test beam setup, we installed a final beam path similar to the test beam. We measured positional fluctuations of this beam path and found them to be at the same level. We then aligned this beam to the ion.

We measured the short-term intensity fluctuations of the beam to be below the 1% level; however, a slow drift of several percent in the beam power was observed. We installed a commercially available noise eater but found that this device did not meet our requirements. We instead decided to build our own power stabilization system (Figure 2). A beam sampler directs a small fraction of the incident power to a photodiode. This photodiode signal is sent to a fast PID feedback controller, which adjusts the modulation amplitude of the RF signal driving an acousto-optic modulator (AOM) to keep the measured optical power constant. After installing this, we measured the intensity fluctuations (Figure 3). The RMS fluctuations were reduced by a factor of 3, and long-term drifts were essentially eliminated. This reduced intensity fluctuations to an acceptable level.

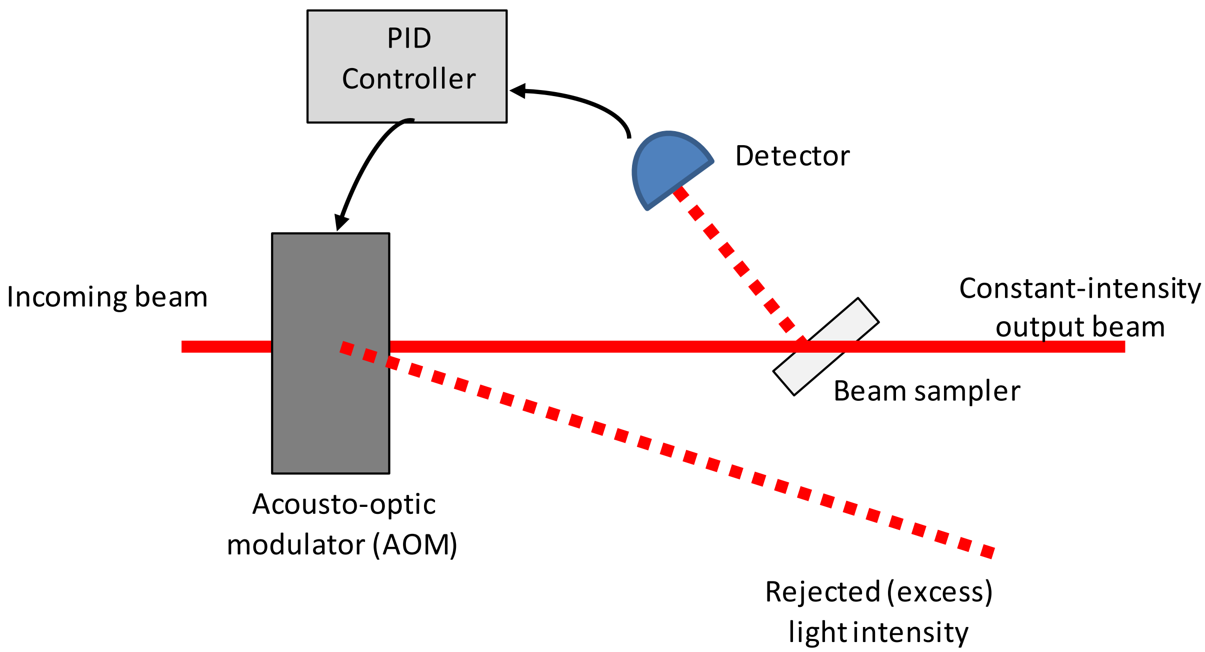

Figure 2. Schematic of power stabilization system setup

These measurements and improvements to the positional and intensity stability of the laser constituted Task I of this program, which is now complete.

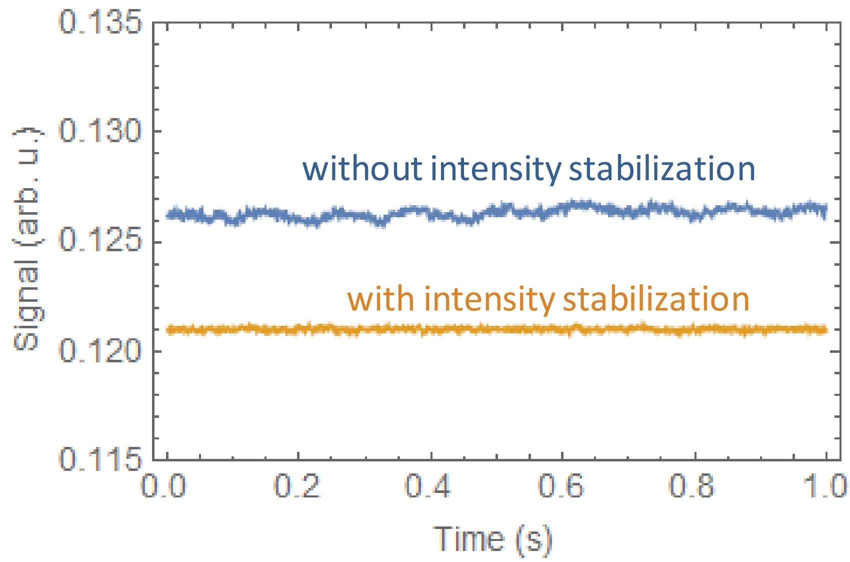

Figure 3. Laser intensity fluctuations with and without laser power stabilization

Task 2

Programming the pulse sequences

Task 2 of the program requires implementation of phase-controlled pulse sequences and successful demonstration of quantum-enhanced imaging, including Heisenberg scaling of the width of the excitation region with pulse length.

To implement the coherent beam pulse sequences, we programmed an AD9910 phase-agile Direct Digital Synthesizer (DDS) chip. We are able to implement pulse sequences of essentially arbitrary length on this chip with a timing resolution of 32 ns. The DDS signal was amplified and sent to an AOM to control the phase and amplitude of the coherent qubit excitation beam at 674 nm. The pulses made in this manner constituted the pulse sequence that enables imaging with Heisenberg scaling when using a coherent target (the ion qubit).

Demonstrations of quantum-enhanced imaging

Figure 4 shows the experimental setup in which we demonstrate quantum-enhanced imaging of a trapped ion. The ion is trapped above a microfabricated surface-electrode trap within an ultra-high-vacuum chamber by a combination of dc and rf fields. A 674-nm laser addresses the coherent transition within the ion, while a 422-nm laser beam is used for readout; fluorescence from the ion is collected by a high numerical aperture lens and detected by a photomultiplier tube (PMT) located below the apparatus.

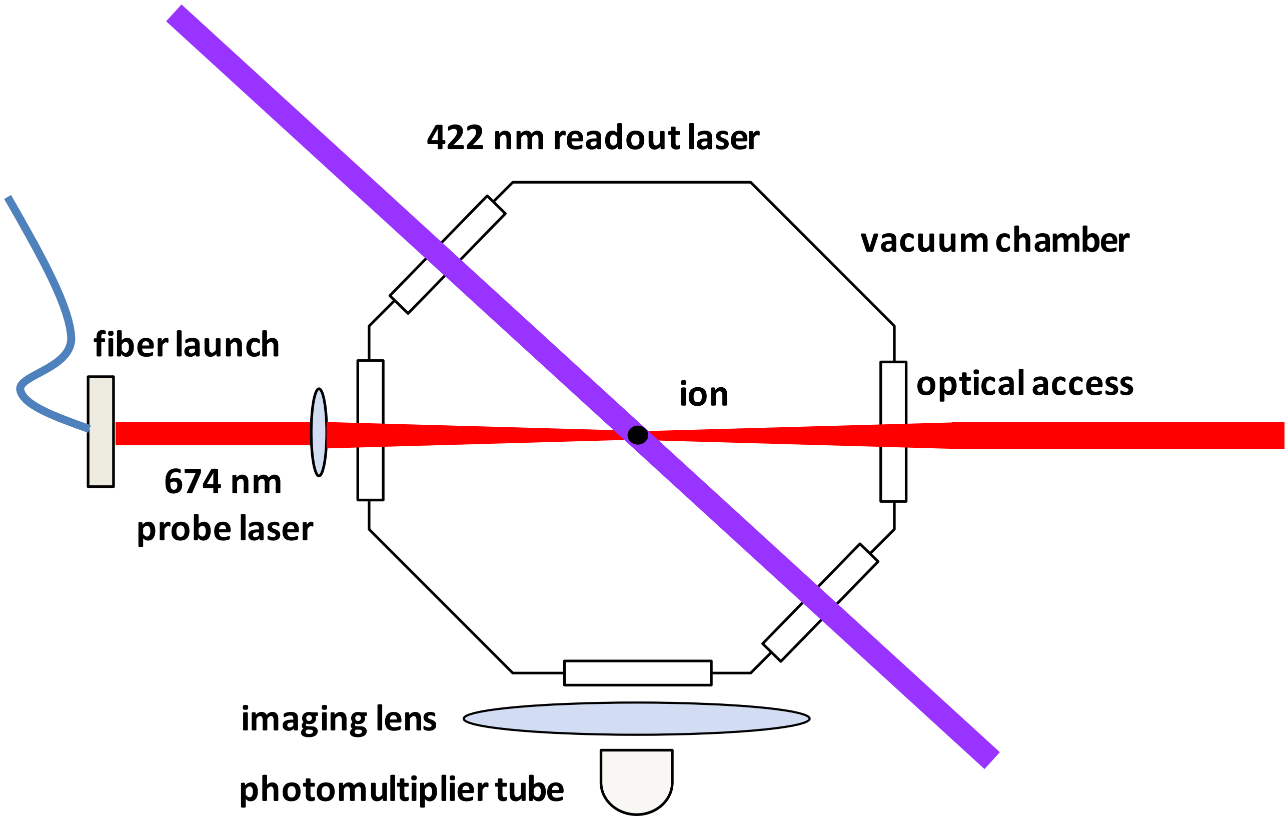

Following implementation of the pulse sequences, we have demonstrated quantum-enhanced imaging of a trapped ion for up to N = 53 pulses (Figure 5). The data demonstrate the (nearly) Heisenberg-limited narrow feature near the center, which sharply narrows with increasing pulse length N, as well as the

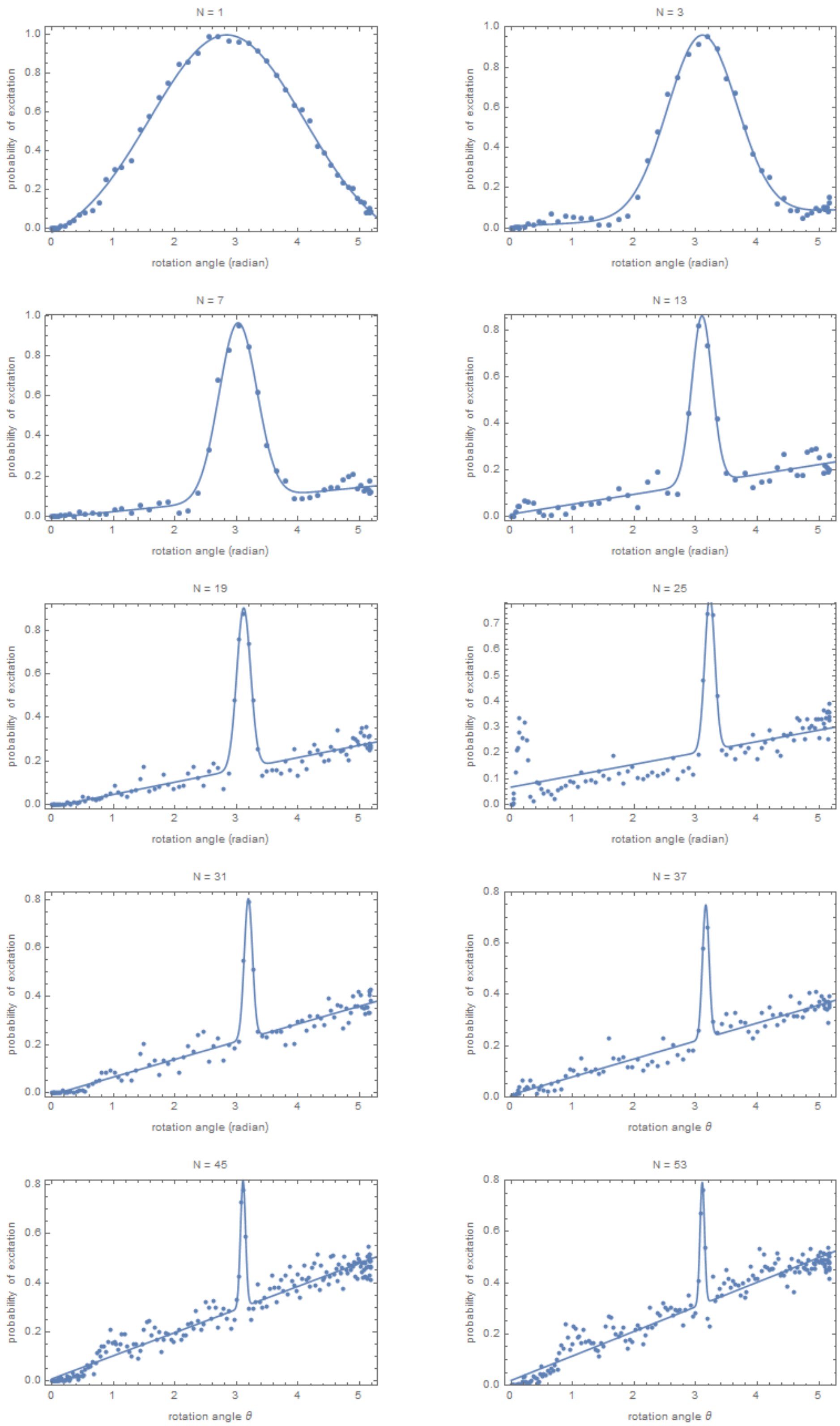

Figure 5. Quantum imaging for pulse sequences of up to $N = 53$ pulses. The width of the excitation region agrees very well with predictions. Background noise due to the imperfect control laser spectrum degrades the performance for high N.

cancellation of excitation at other locations. For N = 53 pulses, the full-width half maximum (FWHM) error is $\Delta\theta$ = 0.15 radians, which corresponds to a relative positional error (as a fraction of beam waist w) of $(\Delta r/w)$ = 3%. This exceeds our program goal of localizing the target to less than 10% of the probe beam width.

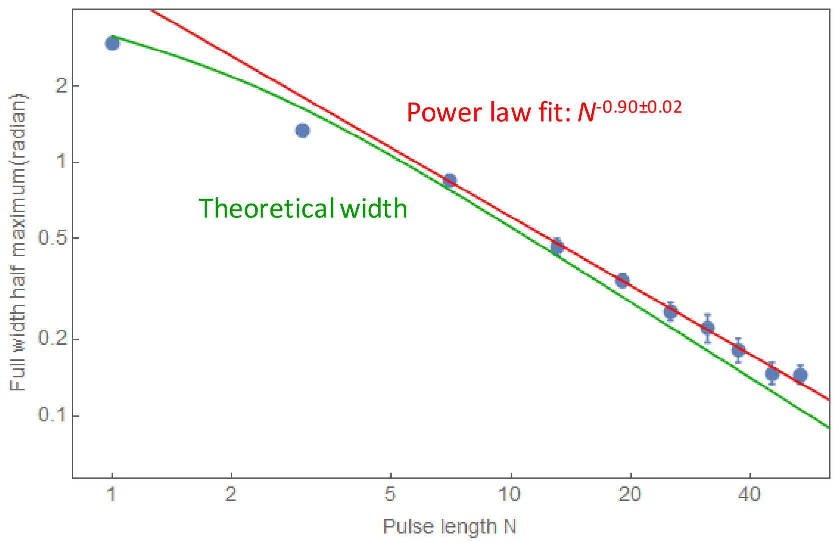

Figure 6. Width of the excitation region (in radians) as a function of pulse length N shows near-Heisenberg-limited scaling going as $N^{-0.90}$

Figure 6 shows the scaling of the full-width half maximum (FWHM) of the excitation peaks as a function of pulse length N. Our measured widths closely agree with the theoretical curve (green curve in Figure 6) although they degrade slightly for the longest pulse sequences. By making a power-law fit to the width of the peak as a function of N (red curve in Figure 6), we find that the central peak width scales as $N^{-0.90 \pm 0.02}$. By comparison, Heisenberg-limited scaling should go as N^{-1}, while classical scaling goes as $N^{-0.5}$. Overall, we come very close to achieving the optimal Heisenberg scaling, the best allowed by quantum mechanics, even for very long pulse sequences.

Figure 5 (previous page) shows that as the length N of the pulse sequence is increased, a noise background which increases with the pulse amplitude (rotation angle) appears. This degrades the performance of the quantum imaging and will prevent use of the binary search algorithm (required for unambiguous target location with Heisenberg scaling) for the largest N, as there will be a significant proportion of “false positive” signals which prevent accurate location of the target. This background is less of a problem for small N and can be dealt with by standard, classical error correction (i.e., repeating the experiment a few times and taking a majority vote of results from the repetition). We developed a numerical model for this degradation, which takes into account the imperfect spectrum of our control laser. This model accurately reproduces our data both for quantum-enhanced imaging and for standard quantum control sequences such as Rabi flopping or Ramsey measurements. In particular, we now understand that the signal degradation we observe for long pulse sequences is specifically due to our laser and is not an inherent limitation of the technique.

These data show that we are able to demonstrate the essential features of quantum-enhanced imaging: a central, narrow peak whose width scales nearly at the Heisenberg limit; unambiguous cancellation of the excitation outside of the central region, and localization of the target to within better than 10% (3% achieved) of the beam width. Furthermore, we are able to understand the limitations of our experimental implementation of the technique. These steps constitute completion of Task 2.

Task 3

Task 3 of the project requires demonstrating the "binary search" algorithm to locate the ion. This algorithm takes advantage of quantum-enhanced imaging to efficiently locate a target which is initially at an unknown location within the beam width.

To implement the binary search, we begin with the ion positioned somewhere within the waist of the control beam, but at an initially unknown location. We then vary the amplitude of the control beam to determine the ion's location within the control beam. By starting with short (broad) pulse sequences and successively increasing the pulse length, we efficiently determine the ion's location to within < 10% of the control beam width.

Implementation of the binary search technique is shown in Figure 7. We begin with an ion of unknown location in the positive half-space of the control beam. A short sequence of length L_1 is applied to the ion for a number n repetitions; if the fraction of times the ion is driven to the excited state ("successes") is greater than some threshold T, the ion is considered to be located in that region of the search space. The number of pulses is then increased to $L_2 > L_1$, and the experiment iterated until the desired resolution is reached. Figure 7 shows four iterations of the binary search for a trapped ion with $n = 9$, $T = 0.5$, $L_1 = 3$ to $L_4 = 17$ pulses. After completion of the binary search algorithm with these parameters, the ion is localized to within only 3% of the initial beam diameter. We thus greatly exceed the program goal of localizing the ion to within 10% of the beam diameter.

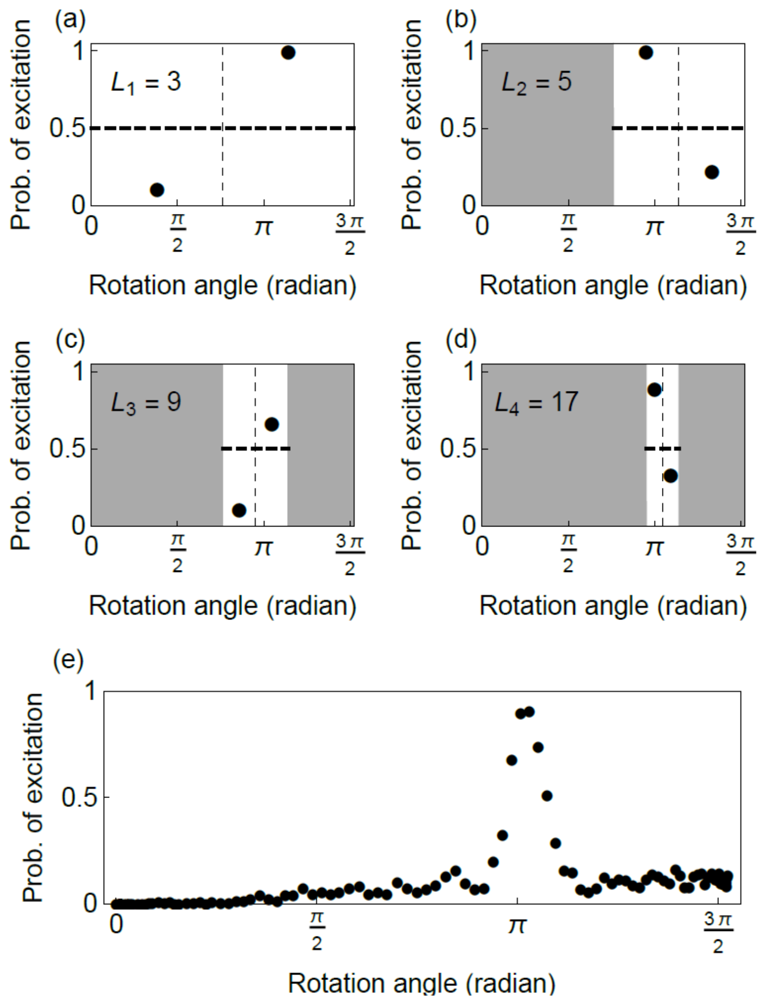

Figure 7. Demonstration of the binary search technique for a coherent target of unknown location. (a) – (d) Here are shown four iterations of the binary search technique, starting from $L_1 = 3$ pulses per sequence to $L_4 = 17$ pulses per sequence. Gray areas represent those regions excluded by previous iterations of the search. The fourth iteration localizes the target to within 3% of the beam diameter. In (e), a full scan with $L_4 = 17$ pulses confirms the location of the trapped ion.

Task Summary (Theoretical)

As part of the theoretical support for this program, we have developed a new family of closed-form broadband 'Optimal Bandwidth' (OB1) pulse sequences. Whereas the pulse sequences used for the Quantum-Enhanced Imaging project are optimally selective in the Rabi frequency of the drive field, these Optimal Bandwidth sequences are optimally unselective. That is, they can implement arbitrary single-qubit rotations with high fidelity on qubit ensembles despite large spatial inhomogeneity in drive fields. These OB1 sequences have applications in quantum control, where they can be used to eliminate the effects of a spatially-varying drive intensity or of slow drifts of drive amplitude without the need for time-consuming error correction protocols.

Similar sequences can be found in the literature, notably the state-of-art sequence known as BB1 which optimizes for a quantity known as maximal flatness. However, our OB1 sequences, which are of the same length, directly optimize for bandwidth of high-fidelity operation (Figure 8), which is often the relevant experimental quantity of interest. In doing so, these OB1 sequences achieve a factor of 16 improvement in infidelity over BB1 given any target inhomogeneity bandwidth in amplitude errors.

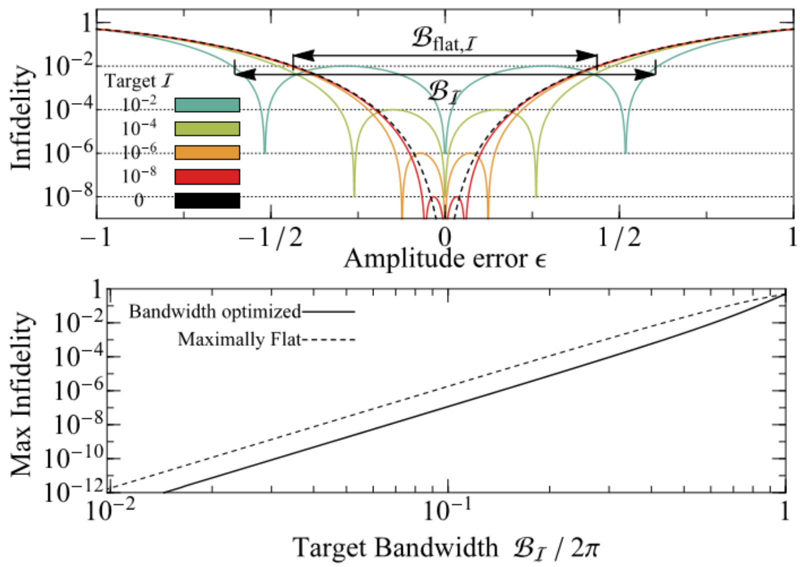

Figure 8. (top) Theoretical Infidelity of various OB1 sequences optimized for implementing π gates with worst-case infidelity I across the widest range of amplitude error inhomogeneity. (bottom) Comparison of OB1 worst-case infidelity (thick) with state-of-art BB1 (dashed).

Future Work

There are at least two scenarios in which quantum-enhanced imaging shows promise. One is long-range radar imaging of a coherent target, which might be a solid-state coherent system (such as a diamond-NV center device) that has been attached to a target of interest. The second is to use quantum-enhanced imaging as a way to achieve site-specific addressing in a qubit system. Here we look at some of the technical requirements for the two applications.

Long-range radar imaging of coherent targets

Quantum-enhanced imaging has the capability to allow superior scaling of long-range radar imaging of coherent targets. Figure 9 represents a schematic of such a possible system. We here outline the advantages and potential challenges of such a system.

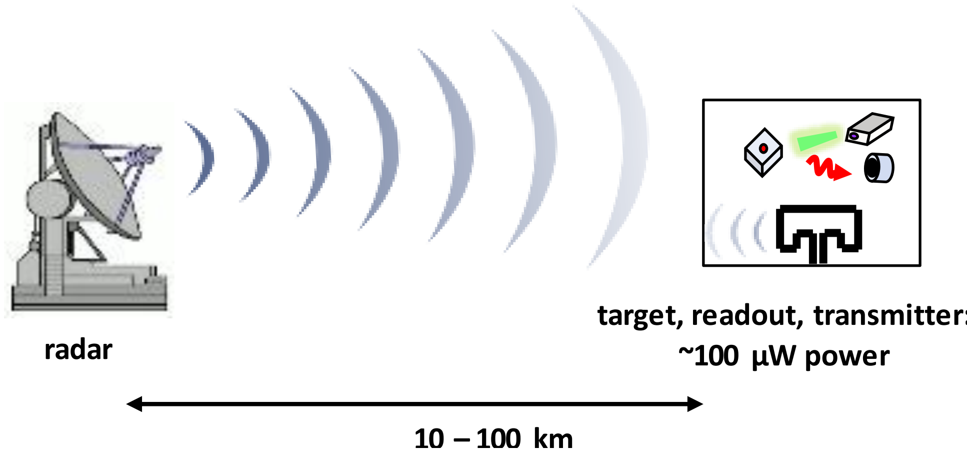

Figure 9. Schematic of a quantum-enhanced imaging system for long-range radar.

The system illustrates a coherent system, possibly a nitrogen-vacancy (NV) center in diamond, attached to a target of interest. The coherent system is illuminated by microwave radiation (the coherent transition in NV centers is in the S band). For diamond-NV centers and other similar quantum systems, no vacuum system or cryogenics is needed to maintain the quantum system and the overhead/system SWAP is thus very low. Only two active components are needed: a low power laser/photodiode system for state readout (required power of a few µW) and a transmitter that sends a signal back to the radar station indicating the quantum state of the target. In order to be above typical detection thresholds, the transmitter need broadcast only small powers (roughly 10s of µW for distances of 10s of km). Depending on distance, the overall power requirements range from 10s to 100s of µW. Using 100 µW as a baseline, the system could be powered continuously for 12 days from a single 300-mg ultralight Li-ion battery. Moreover, the field lifetime would be many months since signal transmission would only be required when the system was actively being queried by a radar. Thus, the quantum system would in fact be a low-overhead, low-SWAP system and could be deployed months in advance of when imaging was actually performed.

It is possible to drive coherent transitions in a quantum system at surprising distances. This is due to the fact that, while incoherent ("classical") transition rates are dependent on the system power and hence decrease rapidly with distance R as $1/R^2$, coherent oscillations depend on the field strength which decreases only as $1/R$. For a radar transmitter of peak power 20 kW and gain of 43 dB, a π-pulse can be driven in a typical S-band transition in about 1 ms from a distance of 10 km away. This is within the coherence time that has been demonstrated for NV centers at room temperature. We thus believe this technique has strong potential for long-range imaging applications.

Nevertheless, extending the coherence time of room-temperature quantum systems is critical to take full advantage of quantum-enhanced imaging. There are two important concerns. First, localizing a target to within a fraction of the beam waist via quantum-enhanced imaging requires many π-pulses to be coherently executed in series. Secondly, the scaling advantage of quantum-enhanced imaging is much greater at larger distances, on the order of 100 km or greater. In fact, at those distances, quantum-enhanced imaging may allow accurate spatial detection of targets that are below the detection threshold for conventional radar. However, to allow many π-pulses to be performed within a coherence time at 100 km , coherence times of 100 ms or greater will be required. These coherence times exist in trapped ion systems, but those quantum systems require much greater overhead. Conversely, coherence times in NV centers at room temperature are currently limited to a few milliseconds. However, these coherence times appear to be impurity-limited and there is reason to believe that they may improve substantially in coming years. We thus recognize that improving the coherence time of these low-overhead, field-ready quantum systems is an essential step towards using quantum-enhanced imaging in a radar application.

Site-selective addressing of qubits within an array

A second promising application for quantum-enhanced imaging is of site-selective addressing of qubits within an array. This application is relevant to scalable approaches to quantum computing and quantum information theory, as the difficulty of individually addressing one out of many qubits is a significant challenge for any quantum computing modality. The pulse sequences, while used for imaging in this program, can equally easily allow for low-crosstalk addressing of a single ion or other quantum target even when that ion is located close to other targets resonant with the same transition. The level of crosstalk can be varied by changing the pulse phases and can be below 10^{-4}.

Quantum-information processing systems already reach many of the requirements to use quantum-enhanced imaging as a method of site-selectivity, as the completion of this program has already shown. In particular, the coherence times of trapped-ion systems are already sufficient to take advantage of this technique, and laboratory control of these quantum systems (initialization, readout, etc.) allows straightforward implementation of this method. An important requirement is to eliminate the deleterious background we observed in our experiments, which would increase the crosstalk seen by non-addressed qubits. However, other research groups have successfully reduced their laser spectral noise by orders of magnitude, most particularly by using an ultrastable cavity as a spectral filter for the coherent excitation light. We have also recently implemented this spectral filtering technique and will soon test its performance. We thus believe that quantum-enhanced imaging may be an enabling technique for scalable quantum information processing.

The next significant step for using the pulse sequences from this program to site-selectively address an array would be to demonstrate selective excitation of one ion within a chain of a few ions via the technique. The Lincoln Laboratory ion-trapping apparatus is configured to allow these experiments, and such results would be immediately applicable in many other quantum-information-processing scenarios.

This material is based upon work supported under Air Force Contract No. FA8702-15-D-0001. Any opinions, findings, conclusions or recommendations expressed in this material are those of the author(s) and do not necessarily reflect the views of the U.S. Air Force.